Transcriptomic evaluation of pulmonary fibrosis-related genes:

utilization of transgenic mice with modifying p38 signal in the lungs

（肺線維化関連遺伝子のトランスクリプトーム解析：

肺 p38 シグナル遺伝子改変マウスの利用）

千葉大学大学院医学薬学府

先端医学薬学専攻

（主任：斎藤 哲一郎 教授、坂尾 誠一郎 准教授）

松田　周一

Abstract: Idiopathic pulmonary fibrosis (IPF) is a progressive fibrosing lung disease that is caused by the dysregulation of alveolar epithelial type II cells (AEC II). The mechanisms involved in the progression of IPF remain incompletely understood, although the immune response accompanied by p38 mitogen-activated protein kinase (MAPK) activation may contribute to some of them. This study aimed to examine the association of p38 activity in the lungs with bleomycin (BLM)-induced pulmonary fibrosis and its transcriptomic profiling. Accordingly, we evaluated BLM-induced pulmonary fibrosis during an active fibrosis phase in three genotypes of mice carrying stepwise variations in intrinsic p38 activity in the AEC II and performed RNA sequencing of their lungs. Stepwise elevation of p38 signaling in the lungs of the three genotypes was correlated with increased severity of BLM-induced pulmonary fibrosis exhibiting reduced static compliance and higher collagen content. Transcriptome analysis of these lung samples also showed that the enhanced p38 signaling in the lungs was associated with increased transcription of the genes driving the p38 MAPK pathway and differentially expressed genes elicited by BLM, including those related to fibrosis as well as the immune system. Our findings underscore the significance of p38 MAPK in the progression of pulmonary fibrosis.

Keywords: p38 mitogen-activated protein kinase; bleomycin-induced pulmonary fibrosis; idiopathic pulmonary fibrosis; RNA sequencing; alveolar epithelial type II cells

---

1. Introduction

Pulmonary fibrosis is the result of the end-stage pathological development of existing lung diseases caused by infection, autoimmunity, chronic inflammation, and idiopathy. Idiopathic pulmonary fibrosis (IPF), one of the most common causes of interstitial pneumonia, is characterized by progressive and irreversible fibrotic scar formation in the gas

exchange regions of the lung, resulting in organ malfunction. IPF is a devastating lung disease as patients show poor prognosis, with a median survival of 2–5 years as well as increased risks of pulmonary hypertension and lung cancer [1]. A chronic inflammatory process of the lung has long been considered a main potential mechanism underlying IPF [2]. Moreover, innate and adaptive inflammation may contribute to determining the rate of disease progression in patients with IPF [3]. However, the mortality of patients with IPF is correlated with the extent of fibrotic focus formation, which results from the abnormal and excessive accumulation of extracellular matrix (ECM) components, including collagen, fibronectin, and elastin [4]. Hence, recent studies focusing on the behaviors of ECM-producing myofibroblasts in pulmonary fibrosis may also inform the identification of therapeutic options for IPF [5–8]. In terms of current pharmacological therapies for IPF, while nintedanib and pirfenidone have been approved by the Food and Drug Administration, neither can improve the survival of patients with IPF [9]. Indeed, new beneficial strategies that enable patients with IPF to survive longer and with improved quality of life have been long-awaited.

Among mitogen-activated protein kinases (MAPKs), members of the p38 MAPK family are activated in response to environmental stresses such as inflammatory stimuli by cytokines and Toll-like receptor ligands, osmolality shock, ultraviolet irradiation, oxidative stress, chemotherapeutic drugs, etc. Of the four isoforms (α, β2, γ, and δ) of p38, p38α is ubiquitously expressed in adult tissues and its physiological and pathological roles have been well investigated [10]. p38 MAPKs are activated by dual phosphorylation of the TGY motif within their activation loop by two upstream MAPK kinases (MAP2Ks)— mitogen-activated protein kinase kinase (MKK)-3 and MKK6—that are activated by various types of MAPKK kinases (MAP3Ks) [11]. In addition to this canonical activation pathway, specific binding of transforming growth factor (TGF)-β-activated kinase 1-binding protein 1 to p38α leads to p38α autophosphorylation and activation [12]. TGF-β signaling is one of the most crucial factors in the murine pulmonary fibrosis model and may be potentiated in the pathogenesis

of IPF [13,14]. These findings strongly suggest the involvement of p38 signaling in the development of pulmonary fibrosis. In fact, several studies have reported that p38 inhibitors, SB239063 and FR-167653, can ameliorate bleomycin (BLM)-induced pulmonary fibrosis [15,16]. Lipopolysaccharide-induced epithelial-mesenchymal transition (EMT), in the early pulmonary fibrosis process, may be associated with p38 and TGF-β/smad3 signaling pathways [17]. Additionally, macrophage-specific loss of function of forkhead box M1, which inhibits the p38 signaling pathway, exacerbates BLM-induced pulmonary fibrosis [18]. Furthermore, pirfenidone was originally recognized as a small molecule p38γ inhibitor that blocks the synthesis of TGF-β [19]. Hence, the involvement of p38 signaling in the pathogenesis of pulmonary fibrosis is indubitable.

Here, we designed the study to elucidate new therapeutic target genes for IPF based on the notion that p38 positively regulates the development of pulmonary fibrosis. Mice with stepwise changes in the intrinsic activity of p38, specifically in alveolar epithelial type II cells (AEC II), were subjected to the pulmonary fibrosis model by BLM because AEC II could play a critical role in the progression of IPF [20]. RNA sequencing of total RNA derived from the lungs followed by transcriptome analysis was performed.

2. Results

2.1. Aggravation of BLM-Induced Murine Pulmonary Fibrosis Correlated with Increased Intrinsic p38 Activity in the Lungs

Histopathological assessment revealed that worsening severity of pulmonary fibrosis was associated with increased intrinsic p38 activity in the lungs (Figure 1A,B). At 8 days post-instillation (dpi) of BLM, tissue infiltration of inflammatory cells and thickening of the alveolar interstitium involved in aberrant collagen accumulation were observed. Moreover, these changes proceeded to diffuse and multifocal distributions at 15 dpi. These histopathological findings of BLM-induced pulmonary fibrosis in the MKK6-constitutive

active (MKK6-CA) group were more severe and extensive than those in the wild-type (WT) group, whereas those in the p38-dominant negative (p38-DN) group were less severe and extensive than those in the WT group. Moreover, the distinct severity of pulmonary fibrosis was evident in semi-quantitative evaluation assessed by a modified Ashcroft score and stratified by three mouse groups. In contrast, no apparent inflammatory and fibrotic changes were observed in phosphate-buffered saline (PBS)-treated groups.

In addition, total cell counts in bronchoalveolar lavage fluid (BALF) at 8 dpi of BLM tended to increase with increased intrinsic p38 activity in the lungs (Figure 1C). Regardless of mouse genotype, macrophages and lymphocytes accounted for approximately 50% and 30% of the total cells in the BALF of BLM-treated groups, respectively (Supplementary Figure S1). Similarly, comprehensive protein analysis in BALF by western blot array revealed 77 upregulated molecules that were evoked by BLM and were associated with increased p38 activity in the lungs (Supplementary Table S1). These upregulated molecules included many pro-inflammatory and pro-fibrotic mediators such as interleukin (IL)-13, IL-17, stromal cell-derived factor 1(SDF-1)/C-X-C motif chemokine ligand (CXCL)-12, interferon (IFN)-γ, keratinocyte chemoattractant (KC)/CXCL1, monokine induced by gamma interferon (MIG)/CXCL9, macrophage inflammatory protein-1α (MIP-1α)/CC chemokine ligand (CCL)-3, and regulated upon activation normal T cell expressed and secreted (RANTES)/CCL5.

Measurements of collagen and static compliance in the lungs also supported the morphological alterations in the three mouse groups treated with BLM (Figure 1D,E). The amount of collagen in the left lungs at 8 dpi in the MKK6-CA group was significantly higher than that in the WT and p38-DN groups, although the difference between the WT and p38-DN groups was not significant. The decrease in static compliance in the MKK6-CA and WT groups was significantly larger than that in the p38-DN group, although the difference was not significant between the MKK6-CA and WT groups. Additionally, a reduction in body

weight tended to increase with increased p38 signaling in the lungs, exhibiting the systemic effect implicated in the severity of BLM-treated mice (Figure 1F).

We verified the differences in intrinsic p38 activity in the lungs that underlie the different severity of BLM-induced fibrosis among three mouse genotypes. Immunofluorescence staining revealed the presence of AEC II, macrophages, and other parenchymal cells expressing p38 in the PBS-treated lungs (Supplementary Figure S2A). The differences in p38 expression in these lung cells were not observed among three mouse groups. In contrast, the proportion of the lung cells showing the nuclear localization of phospho-p38 (P-p38) was increased by BLM treatment (Supplementary Figure S2B,C). Additionally, the increased proportion corresponded with the theoretical stepwise upregulation of intrinsic p38 activity in the lungs, and this finding was most prominent in AEC II. Although p38 is ubiquitously expressed in the cytoplasm of resting cells, activated p38 is represented by the phosphorylation-dependent nuclear localization of p38 in response to various types of stimulation such as DNA damage [21,22]. Therefore, these results demonstrate the three graded intensities of p38 activation induced by BLM among three different mouse genotypes.

2.2. Comparative Transcriptome Analysis of a BLM-Induced Pulmonary Fibrosis Model Exhibiting Different Severity Due to p38 Activity in the Lungs

RNA sequencing (RNA-seq) was performed using lung samples at 8 dpi when the severity of BLM-induced pulmonary fibrosis was apparently different among the three groups and transcriptomic changes in the BLM-induced fibrosis model are more likely to be correlated with the progression of IPF [23,24]. Principal component analysis (PCA) showed a relationship in the expression of genes among the three mouse groups treated with BLM and PBS, while hierarchical clustering analysis visualized using a heatmap highlighted the trend of differentially expressed genes (DEGs) between the BLM- and PBS-treated groups (Figure 2A). In the PCA plot, the BLM-treated groups were all well separated from the PBS-

treated groups and the variance in BLM-treated groups was less than that in PBS-treated groups, indicating the assembly of distinct clusters following BLM exposure. Consistent with this observation, hierarchical clustering analysis identified DEGs between the BLM- and PBS-treated groups. Gene set enrichment analysis (GSEA) in the p38 MAPK pathway revealed that genes involved in regulating this pathway were significantly upregulated in the BLM-treated WT and MKK6-CA groups compared to those in the PBS-treated group (false discovery rate [FDR] q value < 0.25) but not in the p38-DN group (Figure 2B). Moreover, volcano plots in the three mouse groups showed that the increased number of DEGs between the BLM- and PBS-treated groups was associated with an increase in p38 signaling in the lungs (Figure 2C). BLM treatment upregulated approximately two-fold more DEGs and downregulated 2.5-fold more DEGs in the MKK6-CA group than those in the p38-DN group.

Next, we performed transcriptome analysis to detect the enriched functions of DEGs driven by BLM treatment. K-means clustering followed by Kyoto Encyclopedia of Genes and Genomes (KEGG) pathway enrichment analysis revealed the enriched pathways of four clusters in DEGs between the BLM- and PBS-treated groups of three mouse genotypes (Figure 3A). These pathways included fibrosis-related pathways such as protein processing in endoplasmic reticulum (ER) (yellow cluster), cytokine–cytokine receptor interaction (purple cluster), and ECM–receptor interaction (purple and green clusters) in addition to pathways related to immune systems such as hematopoietic cell lineage and leukocyte transendothelial migration. In contrast, we identified 493 common DEGs upregulated by BLM among the three mouse groups (Figure 3B and Supplementary Table S2). Regarding 493 common upregulated DEGs, enrichment analysis by gene ontology (GO) revealed three ECM-related annotations among the top five enriched molecular functions and all five terms associated with immune systems among the top five enriched biological processes. Additionally, the cytokine–cytokine receptor interaction was the most significantly enriched pathway among the top five KEGG pathways.

2.3. Exploration of Novel Potential Genes Contributing to the Progression of Pulmonary Fibrosis

To identify the pathogenetically relevant genes in the progression of IPF, we investigated the correlation of upregulated genes between BLM-induced fibrotic lungs showing the three different severity levels and human IPF lungs (Figure 4). In the BLM-treated groups, K-means clustering analysis identified a cluster of 2722 genes that their mean reads per kilobase of exon per million mapped sequence reads (RPKM) values increased along with stepwise elevation of p38 signaling in the lungs. We verified 137 DEGs that were included in this cluster and upregulated in common with the three BLM-treated mouse groups. Additionally, human RNA-seq data that provided 475 upregulated DEGs in IPF lung tissue compared to healthy lung tissue was obtained from the Gene Expression Omnibus website (accession ID: GSE52463). Finally, comparison of our data with human RNA-seq data identified four overlapping DEGs; namely, EPH receptor A3 (*EPHA3*), POU class 2 homeobox associating factor 1 (*POU2AF1*), SAM domain, SH3 domain and nuclear localization signals 1 (*SAMSN1*), and ectodysplasin A2 receptor (*EDA2R*).

3. Discussion

This study investigated the molecular mechanisms involved in the progressive worsening of BLM-induced pulmonary fibrosis in three genotypes of mice carrying stepwise variations of p38 activity in AEC II. We demonstrated that BLM-induced severe inflammation and fibrosis that was correlated with increased p38 activity in the lungs. Transcriptome analysis of this model provided a connection between the progression of pulmonary fibrosis and genes driving ER functions, ECM-cell interaction, and the immune system. Moreover, we identified candidate genes associated with IPF progression in comparison to a publicly available IPF dataset. The results of these comprehensive analyses suggest that the progression of pulmonary fibrosis occurs concurrently with increased p38

activity in AEC II, which provokes the enhancement of inflammation and immune systems. Therefore, this novel model of pulmonary fibrosis serves as a tool for understanding IPF progression.

Addressing the mechanisms contributing to IPF progression can lead to improved prognosis as this complex multi-pathway disease shows heterogeneity in its clinical course [1,4]. The present study applied a severe model of BLM-induced pulmonary fibrosis to study disease progression. Although the BLM-induced pulmonary fibrosis model is insufficient to mimic the pathogenesis of IPF, it has shown high reproducibility and the important mechanisms of pulmonary fibrosis, such as epithelial-mesenchymal crosstalk and TGF-β signaling pathway [25,26]. BLM-induced pulmonary fibrosis shows a transition from the inflammatory to the fibrotic phase at around 7 dpi, establishment of fibrosis at 14 dpi, and subsequent formation of reversible lesions [27,28]. In this context, the analyses were mainly conducted at 8 dpi as the optimal timing to evaluate the progression of pulmonary fibrosis. Additionally, the transcriptome profiling approach enables us to reveal the molecular mechanisms regulating fibrosis in this model and compare them to the profiles in the lung samples of IPF patients. Recent studies have shown that variations in gene expression of BLM-induced pulmonary fibrosis were correlated with changes in IPF severity [23,24]. Notably, the genes differentially expressed in BLM-induced pulmonary fibrosis are most abundant in the active fibrotic phase (7–14 dpi), which shows the highest correlation with IPF lung samples [23,24]. This finding explains the rationale that the gene expression profiles of BLM-treated lungs are altered before remarkable changes in morphology and function occur. Taken together, these findings are compatible with our study, which has implications for the development of pulmonary fibrosis in transcriptome analysis.

Although apoptosis and reprogramming of lung epithelial cells play a prominent role in IPF, the molecular details remain uncertain [20,29]. p38 is required for maintaining AEC II homeostasis as a physiological function, whereas extracellular stimuli-mediated

enhancement of p38 is attributed to lung inflammation and immune responses and is associated with apoptosis in AEC II [30,31]. We focused on p38 activity in AEC II to examine pulmonary fibrosis progression and performed transcriptome analysis. The results showed distinct expression of p38 MAPK pathway genes that was positively correlated with stepwise changes in intrinsic p38 activity in the lungs and the contribution of the immune system and ER functions to the development of pulmonary fibrosis mediated by activation of the p38 MAPK pathway. Regarding lung inflammation, the exacerbation correlated with increased p38 activity in the AEC II manifested as increases in inflammatory cells and pro-inflammatory cytokines in BALF and the enrichment of genes facilitating immune cell infiltration and cytokine interaction pathways. Augmentation of pro-fibrotic cytokines and immune response arising from inflammation leads to progression of tissue remodeling and fibrosis in the lungs [32]. In particular, the TGF-β signaling pathway driven by p38 induces EMT and fibroblast proliferation and activation through epithelial–mesenchymal crosstalk [33–35]. In this study, TGF-β1 was included in the 137 overlapping genes that showed correlations with intrinsic p38 activity in the lungs and upregulation among the three mouse groups treated with BLM (Figure 4 and Supplementary Tables S2). Additionally, IL-13 and IL-17, which in BALF were upregulated with a concomitant increase in intrinsic p38 activity in the lungs, can promote TGF-β signaling pathway-dependent EMT and fibroblast proliferation and resistance to apoptosis [36,37]. These cytokines originate from immune cells such as T cells, suggesting an association between the immune system and fibrosis [38,39]. A previous study showed that increased immune cells and aberrant regenerating epithelial cells express inflammatory mediators, including IL-17, in active fibrotic lesions of IPF lungs [40]. Furthermore, single-cell RNA-seq analysis of epithelial cells displaying atypical phenotypes in IPF lungs showed that these epithelial cells modulated the expression of inflammatory response- and TGF-β signaling pathway-related genes, leading to fibrotic remodeling [41]. Collectively, these findings strongly suggest that inflammation and immune

response enhanced by increased p38 activity in AEC II may contribute to the fibrotic process in the lungs.

Another possible explanation for the mechanism affecting fibrosis is that maladaptive ER stress response and its mediated apoptosis occurred concomitantly with increased p38 activity in AEC II. ER functions to retain cellular homeostasis by conducting posttranslational modification of proteins, with an adaptive process called unfold protein response under various stress conditions, although an excess of ER stress disrupting this adaptation elicits apoptosis [42]. The enrichment analysis in our study revealed that the ER protein processing pathway activated by BLM-induced reactive oxygen species was correlated with increased p38 activity in the AEC II. This result is consistent with the fundamental principle that ER stress can function in concert with the p38 MAPK pathway [43]. Simultaneously, AEC II homeostasis is sustained by its interaction with ECM, and p38 may participate in it [44]. A recent study using human fibroblasts revealed that the p38 MAPK pathway mediated the acquired resistance of ER stress modified by ECM metabolism through cell-to-ECM interaction [45]. In our study, ECM-receptor interaction was also a pathway enriched in accord with increased p38 activity in AEC II. Moreover, upregulation of ECM-related genes in enrichment analysis and matrix metalloproteases (MMPs; MMP-2, -3, and -9) in BALF (Supplementary Table S1), in addition to higher amounts of collagen, were connected to increased p38 activity in AEC II. These results are consistent with the study that MK2, a downstream substrate of p38, engaged in fibroblast activation and ECM production potentiated by fibroblast activation [46]. In addition, MMPs, which degrade all components of the ECM, are regulated by p38, while their upregulation leads to apoptosis and abnormal regeneration of lung epithelial cells [47]. Hence, ER stress in AEC II can be augmented by not only BLM-induced cytotoxicity, but also by the accumulation of ECM and AEC II to ECM interaction, controlled by the p38 MAPK pathway. These results emphasize the importance of p38 activity in AEC II and its related molecules in the progression of

pulmonary fibrosis. In contrast, this murine model created by the intratracheal administration of BLM was not followed up after the establishment of pulmonary fibrosis. Therefore, further studies are required to determine whether p38 activity in AEC II influences the restoration of BLM-induced pulmonary fibrosis.

We validated four therapeutic target genes by comparing our data with publicly available data from IPF patients. First, *EPHA3* is expressed predominantly in lymphocytes and encodes a receptor tyrosine kinase implicated in regulating cell adhesion and cellular motility [48]. A recent study demonstrated that a novel epithelial cell population derived from IPF lungs co-expressed EPHA3 and CC chemokine receptor (CCR)-10 and facilitated the development of lung remodeling [49]. CCL28, a chemokine ligand for CCR10, was upregulated in BALF in accordance with increased p38 activity (Supplementary Table S1) [50]. These findings suggest that coordination between CCL28-CCR10 chemokine signaling and the p38 MAPK pathway has important implications for reprogramming of epithelial cells, a speculation that warrants further investigation. Second, *POU2AF1* encodes a transcriptional coactivator that regulates B cell maturation and humoral immunity and is expressed in both airway epithelial and B cells [51,52]. A prior study using IPF lungs documented that transcriptome analysis identified *POU2AF1* as a promoter of pulmonary fibrosis and it is highly expressed in aggregates of B cells [53]. Third, *EDA2R* regulates ectodermal tissue development; its expression in lung epithelial cells such as AEC II was ascertained by single-cell RNA-seq data set in IPF lungs [41,54]. Genome-wide association study using human lung tissue identified *EDA2R* as a candidate gene involved in lung aging [55]. In addition, this gene accelerates the apoptotic process in two different types of epithelial cells by activation of p53 signaling and caspase cascade [56,57]. These findings suggest the involvement of *EDA2R* in AEC II senescence and apoptosis. Lastly, *SAMSN1* is expressed in healthy lung epithelial cells but not in lung cancer cells [58]. Although its functions in the lungs remain unknown, this gene is pivotal in regulating B cell activation and differentiation [59]. Thus, changes in

the expression levels of these candidate genes by p38 activity may be involved in promoting fibrosis through molecular interactions between epithelial and immune cells in the IPF lung. This hypothesis is supported by two previous reports showing an association of lymphocytes and epithelial cells with progressive fibrosis in transcriptome analysis of IPF lungs [60,61]. Therefore, the interplay between these genes and the p38 MAPK pathway may be key to understanding the immunological mechanisms underlying IPF progression. However, further studies are needed to confirm the clinical significance of these genes in the patients with rapidly progressive IPF.

4. Materials and Methods

4.1. Mice

All animal procedures conformed to the Japanese regulations for animal care and use, following the Guidelines for Animal Experimentation of the Japanese Association for Laboratory Animal Science. Male and female C57BL/6J mice were purchased from Clea Japan (Tokyo, Japan). Using the 3.7SP-C/SV40 vector kindly provided by Dr. Jeffrey A. Whitsett (Children's Hospital Medical Center, Division of Pulmonary Biology, Cincinnati, Ohio), we generated the following transgenic mice: C57BL/6J-hSP-C-M2 flag-p38α dominant-negative (d.n., dual mutations in wild mouse p38α: Thr180 to Ala; Tyr182 to Phe) TG (p38-DN) mice [62] and C57BL/6J-hSP-C-3HA-tag-MKK6 constitutive-active (c.a., dual mutations in wild human MKK6: Ser207 to Asp; Tyr211 to Asp) TG (MKK6-CA) mice [63]. We confirmed that each transgene-derived product was expressed at least in surfactant protein C (SP-C)-positive AEC II in the lung by using anti-M2-Flag or anti-HA tag antibody. Male heterozygous TG mice and WT littermates aged 10–12 weeks were used for the experiments. The animals were housed in standard laboratory cages and allowed food and water throughout the experiments. The studies were performed according to a protocol approved by the Committee of Animal Welfare of Chiba University.

4.2. BLM-Induced Pulmonary Fibrosis Model

Mice were anesthetized and the neck skin of each was cut longitudinally to expose the trachea. After a single intratracheal instillation of BLM hydrochloride (3 mg/kg; Nippon Kayaku, Tokyo, Japan) dissolved in PBS using a repeating syringe dispenser (Hamilton, Reno, NV, USA), the skin was sutured. Control mice were administered a sham treatment with PBS. Then, changes in body weight were measured daily. To evaluate the histopathological changes in the lung samples at 8 and 15 dpi of BLM, freshly cut lung sections (5 μm thick) were placed on adhesive glass slides (Matsunami Glass Ltd., Osaka, Japan) and stained with Masson's trichrome. The changes in the fibrotic lung samples were evaluated semi-quantitatively according to the modified Ashcroft method with a scoring grade of 0 to 8 [64]. In addition, the collagen content of the left lung was measured using the Sicol Soluble Collagen Assay Kit (Biocolor Life Science Assays, Carrickfergus, United Kingdom) according to the manufacturer's protocol.

4.3. Evaluation of Inflammatory Cells in BALF

At 8 dpi, the trachea was exposed and lavaged three times with 1 mL ice-cold PBS using a 20-gauge catheter. The BALF was centrifuged at 400 × g for 10 min and the resulting supernatants were stored at −80°C for protein array analysis. The resulting cell pellets were resuspended in PBS and subjected to cell counting using a hemocytometer in combination with Diff-Quick (Sysmex Corporation, Kobe, Japan) staining.

4.4. Measurement of Left Lung Compliance

As described previously [65], the lung compliance of the mice was measured by drawing static air pressure–volume relationships in a mixture of medetomidine, midazolam, and butorphanol (M/M/B: 0.3/4/5 mg/kg)-anesthetized mice tracheotomized with polyethylene tubing (O.D. = 0.8 mm). Total lung capacity was defined as the lung volume of full inflation

judged by visual inspection of the lung that fully occupied the chest cavity. Functional residual volume was defined as deflation at 0 cmH_2O. Lung volumes at an airway pressure of 20 cmH_2O were estimated between mice at 8 dpi with BLM and PBS in the three genotypes (WT, p38-DN, and MKK6-CA mice).

4.5. Immunofluorescence Staining

The lung sections were pretreated with 1:10 FcR blocking agent (Miltenyi Biotech, Gladbach, Germany) for 10 min. They were then treated with primary antibodies (1:100 dilution) as follows: goat anti-proSP-C polyclonal antibody (sc-7706; Santa Cruz Biotech, Dallas, TX, USA), rabbit anti-p38 polyclonal antibody (original production [66]), rabbit anti-proSP-C antibody (customized production [60]; Sigma-Aldrich Japan Genosys, Ishikari, Japan), and mouse anti-phospho-p38 MAPK (pT180/pY182) (clone30, 612281; BD Biosciences, NJ, USA), followed by staining with appropriate fluorescein-conjugated secondary antibodies (1:200 dilution), and 4′,6-diamidino-2-phenylindole (DAPI) was used for nuclear staining. The stained sections were observed under a fluorescence microscope (Axio Imager A2; Zeiss, Oberkochen, Germany).

4.6. RNA Sequencing

At 8 dpi, mice under anesthesia were intracardially perfused with ice-cold PBS to wash out blood cells in the lungs and sacrificed. The left lung lobes were homogenized in ISOGEN plus (TaKaRa Bio, Kusatsu, Japan), and total RNA was extracted. Thereafter, 500 ng of total RNA was ribosomal RNA-depleted using a NEBNext rRNA Depletion Kit (New England Biolabs) and was converted to Illumina sequencing library using NEBNext Ultra Directional RNA Library Prep Kit (New England Biolabs). The library was validated to determine the size distribution and concentration using a Bioanalyzer (Agilent Technologies). Sequencing was performed on a NextSeq 500 (Illumina) instrument with paired-end 36-base read options. Reads were mapped on the mm10 mouse reference genome and quantified using CLC

Genomics Workbench version 12.0 (QIAGEN). All RNA-seq data sets were deposited in the Gene Expression Omnibus database at the National Center for Biotechnology Information with accession number GSE154074.

4.7. Identification of Differentially Expressed Genes (DEGs)

To estimate the expression patterns of transcripts among the three genotypes (WT, p38α d.n.-TG and MKK6 c.a.-TG mice) with or without BLM instillation, the read counts were normalized by calculating the number of reads per kilobase per million for each transcript in individual samples using CLC Genomics Workbench version 12.0 (QIAGEN) [67]. Filtering characteristics of fold change -2 to 2 (FDR at $p < 0.05$) were used to identify the DEGs. Subsequently, the distinct gene expression patterns were analyzed comparatively through PCA and clustering heatmaps using CLC Genomics Workbench. GSEA for p38 MAPK pathways in the BLM-treated group among the three genotypes was also performed using GSEA_4.0.3. [68]. K-means functional enrichment analysis of DEGs was analyzed using integrated differential expression and pathway analysis (iDEP) online tools [69]. A volcano plot was used to compare the gene expression levels in terms of the $\log_2$ fold change. The GO (molecular function and biological process) and KEGG pathway analyses of DEGs between BLM- and PBS-treated groups were performed using ToppGene Suite (https://toppgene.cchmc.org) [70]. Finally, K-means cluster analysis was performed to identify BLM-upregulated genes that depended on the theoretical intrinsic activity of the p38 signal (p38-DN < WT < MKK6-CA) using CLC Genomics Workbench.

4.8. Statistical Analysis

Data are expressed as means ± standard error of the mean (SEM). Statistical analysis was conducted using GraphPad Prism Version 6 (GraphPad Software, San Diego, CA, USA). Statistical significance was determined by one-way analysis of variance (ANOVA) followed by Tukey's or Student's *t*-tests, and *p*-values < 0.05 were considered significant.

Supplementary Materials: Supplementary Materials can be found at http://www.mdpi.com/1422-0067/21/18/6746/s1.

Abbreviations

AEC II	alveolar epithelial type II cells
ANOVA	analysis of variance
BALF	bronchoalveolar lavage fluids
BLM	bleomycin
CCL	CC chemokine ligand
CCR	CC chemokine receptor
CXCL	C-X-C motif chemokine ligand
DAPI	4′,6-diamidinoA-phenylindole
DEG	differentially expressed gene
dpi	days post-instillation
ECM	extracellular matrix
EDA2R	ectodysplasin A2 receptor
EMT	epithelial-mesenchymal transition
EPHA3	EPH receptor A3
ER	endoplasmic reticulum
FDR	false discovery rate
GO	gene ontology
GSEA	gene set enrichment analysis
HA	hemagglutinin
iDEP	integrated Differential Expression and Pathway analysis
IFN	interferon

IL	interleukin
IPF	idiopathic pulmonary fibrosis
KC	keratinocyte chemoattractant
KEGG	Kyoto Encyclopedia of Genes and Genomes
MAPK	mitogen-activated protein kinase
MAP2K	MAPK kinase
MAP3K	MAPKK kinase
MIP-1α	macrophage inflammatory protein-1α
MIG	monokine induced by gamma interferon
MKK3/6	mitogen-activated protein kinase kinase 3/6
MKK6-CA	MKK6-constitutive active
MMP	matrix metalloprotease
NES	normalized enrichment scores
p38-DN	p38-dominant negative
P-p38	phospho-p38
PBS	phosphate-buffered saline
PCA	principal component analysis
POU2AF1	POU class 2 homeobox associating factor 1
RANTES	regulated upon activation normal T cell expressed and secreted
RNA-seq	RNA sequencing
RPKM	reads per kilobase of exon per million mapped sequence reads
SAMSN1	SAM domain, SH3 domain and nuclear localization signals 1
SDF-1	stromal cell-derived factor 1
SEM	standard error of the mean
SP-C	surfactant protein C
SV40	sarcoma virus 40

TGF	transforming growth factor
WT	wild-type

References

1. Lederer, D.J.; Martinez, F.J. Idiopathic pulmonary fibrosis. *N. Engl. J. Med.* **2018**, *378*, 1811-1823. DOI: 10.1056/NEJMra1705751
2. Crystal, R.G.; Bitterman, P.B.; Rennard, S.I.; Hance, A.J.; Keogh, B.A. Interstitial lung diseases of unknown cause. Disorders characterized by chronic inflammation of the lower respiratory tract. *N. Engl. J. Med.* **1984**, *310*,154–166. DOI: 10.1056/NEJM198401193100304
3. Balestro, E.; Calabrese, F.; Turato, G.; Lunardi, F.; Bazzan, E.; Marulli, G.; Biondini, D.; Rossi, E.; Sanduzzi, A.; Rea, F.; et al. Immune inflammation and disease progression in idiopathic pulmonary fibrosis. *PLOS ONE* **2016**, *11*, e0154516. DOI: 10.1371/journal.pone.0154516
4. Wynn, T.A.; Ramalingam, T.R. Mechanisms of fibrosis: therapeutic translation for fibrotic disease. *Nat. Med.* **2012**, *18*, 1028–1040. DOI: 10.1038/nm.2807
5. Yamazaki, R.; Kasuya, Y.; Fujita, T.; Umezawa, H.; Yanagihara, M.; Nakamura, H.; Yoshino, I.; Tatsumi, K.; Murayama, T. Antifibrotic effects of cyclosporine A on TGF-β1–treated lung fibroblasts and lungs from bleomycin-treated mice: role of hypoxia-inducible factor-1α. *FASEB J.* **2018**, *31*, 3359–3371. DOI: 10.1096/fj.201601357R
6. Rangarajan, S.; Bone, N.B.; Zmijewska, A.A.; Jiang, S.; Park, D.W.; Bernard, K.; Locy, M.L.; Ravi, S.; Deshane, J.; Mannon, R.B.; et al. Metformin reverses established lung fibrosis in a bleomycin model. *Nat. Med.* **2018**, *24*, 1121–1127. DOI: 10.1038/s41591-018-0087-6

7. Penke, L.R.; Speth, J.M.; Dommeti, V.L.; White, E.S.; Bergin, I.L.; Peters-Golden, M. FOXM1 is a critical driver of lung fibroblast activation and fibrogenesis. *J. Clin. Invest.* **2018**, *128*, 2389–2405. DOI: 10.1172/JCI87631
8. Suzuki, K.; Kim, JD.; Ugai, K.; Matsuda, S.; Mikami, H.; Yoshioka, K.; Ikari, J.; Hatano, M.; Fukamizu, A.; Tatsumi, K.; et al. Transcriptomic changes involved in the dedifferentiation of myofibroblasts derived from the lung of a patient with idiopathic pulmonary fibrosis. *Mol. Med. Rep.* **2020**, *22*, 1518–1526. DOI: 10.3892/mmr.2020.11218
9. Raghu, G.; Selman, M. Nintedanib and pirfenidone. New antifibrotic treatments indicated for idiopathic pulmonary fibrosis offer hopes and raises questions. *Am. J. Respir. Crit. Care Med.* **2018**, *191*, 252–254. DOI: 10.1164/rccm.201411-2044ED
10. Rincón, M.; Davis, R.J. Regulation of the immune response by stress-activated protein kinases. *Immunological Rev.* **2009**, *228*, 212–224. DOI: 10.1111/j.1600-065X.2008.00744.x
11. Kasuya, Y.; Umezawa, H.; Hatano M. Stress-activated protein kinases in spinal cord injury: focus on roles of p38. *Int. J. Mol. Sci.* **2018**, *19*, 867. DOI: 10.3390/ijms19030867
12. Ge, B.; Gram, H.; Di Padova, F.; Huang, B.; New, L.; Ulevitch, R.J.; Luo, Y.; Han, J. MAPKK-independent activation of p38α mediated by TAB1-dependent autophosphorylation of p38α. *Science* **2002**, *295*, 1291–1294. DOI: 10.1126/science.1067289
13. Li, M.; Krishnaveni, M.S.; Li, C.; Zhou, B.; Xing, Y.; Banfalvi, A.; Li, A.; Lombardi, V.; Akbari, O.; Borok, Z.; et al. Epithelium-specific deletion of TGF-β receptor type II protects mice from bleomycin-induced pulmonary fibrosis. *J. Clin. Invest.* **2011**, *121*, 277–287. DOI: 10.1172/JCI42090

14. Coker, R.K.; Laurent, G.J.; Jeffery, P.K.; du Bois, R.M.; Black, C.M.; McAnulty, R.J. Localization of transforming growth factor β1 and β3 mRNA transcripts in normal and fibrotic human lung. *Thorax* **2001**, *56*, 549–556. DOI: 10.1136/thorax.56.7.549
15. Underwood, D.C.; Osborn, R.R.; Bochnowicz, S.; Webb, E.F.; Rieman, D.J.; Lee, J.C.; Romanic, A.M.; Adams, J.L.; Hay, D.W.; Griswold, D.E. SB 239063, a p38 MAPK inhibitor, reduces neutrophilia, inflammatory cytokines, MMP-9, and fibrosis in lung. *Am. J. Physiol. Lung Cell. Mol. Physiol*. **2000**, *279*, L895–L902. DOI: 10.1152/ajplung.2000.279.5.L895
16. Matsuoka, H.; Arai, T.; Mori, M.; Goya, S.; Kida, H.; Morishita, H.; Fujiwara, H.; Tachibana, I.; Osaki, T.; Hayashi, S. A p38 MAPK inhibitor, FR-167653, ameliorates murine bleomycin-induced pulmonary fibrosis. *Am. J. Physiol. Lung Cell. Mol. Physiol.* **2002**, *283*, L103–L112. DOI: 10.1152/ajplung.00187.2001
17. Cao, Y.; Liu, Y.; Ping, F.; Yi, L.; Zeng, Z.; Li, Y. miR-200b/c attenuates lipopolysaccharide-induced early pulmonary fibrosis by targeting ZEB1/2 via p38 MAPK and TGF-β/smad3 signaling pathways. *Lab. Invest.* **2018**, *98*, 339–359. DOI: 10.1038/labinvest.2017.123
18. Goda, C.; Balli, D.; Black, M.; Milewski, D.; Le, T.; Ustiyan, V.; Ren, X.; Kalinichenko, V.V.; Kalin, T.V. Loss of FOXM1 in macrophages promotes pulmonary fibrosis by activating p38 MAPK signaling pathway. *PLoS Genet.* **2020**, *16*, e1008692. DOI: 10.1371/journal.pgen.1008692
19. Moran, N. p38 kinase inhibitor approved for idiopathic pulmonary fibrosis. *Nat. Biotech.* **2011**, *29*, 301. DOI: 10.1038/nbt0411-301
20. Parimon, T.; Yao, C.; Stripp, B.R.; Noble, P.W.; Chen, P. Alveolar epithelial type II cells as drivers of lung fibrosis in idiopathic pulmonary fibrosis. *Int. J. Mol. Sci.* **2020**, *21*, 2269. DOI: 10.3390/ijms21072269
21. Gong, X.; Ming, X.; Deng, P.; Jiang, Y. Mechanisms regulating the nuclear translocation

of p38 MAP kinase. *J. Cell Biochem.* **2010**, 110, 1420-1429. doi: 10.1002/jcb.22675

22. Wood, C.D.; Thornton, T.M.; Sabio, G.; Davis, R.A.; Rincon, M. Nuclear localization of p38 MAPK in response to DNA damage. *Int. J. Biol. Sci.* **2009**, 5, 428-437. doi: 10.7150/ijbs.5.428
23. Peng, R.; Sridhar, S.; Tyagi, G.; Phillips, E.J.; Garrido, R.; Harris, P.; Burns, L.; Renteria, L.; Woods, J.; et al. Bleomycin induces molecular changes directly relevant to idiopathic pulmonary fibrosis: a model for "active" disease. *PLoS One.* **2013**, 8, e59348. DOI: 10.1371/journal.pone.0059348
24. Bauer, Y.; Tedrow, J.; de Bernard, S.; Birker-Robaczewska, M.; Gibson, K.F.; Guardela, B.J.; Hess, P.; Klenk, A.; Lindell, K.O.; Sylvie Poirey, S.; et al. A novel genomic signature with translational significance for human idiopathic pulmonary fibrosis. *Am. J. Respir. Cell Mol. Biol.* **2015**, 52, 217–231. DOI: 10.1165/rcmb.2013-0310OC
25. Moeller, A.; Ask, K.; Warburton, D.; Gauldie, J.; Kolb, M. The bleomycin animal model: a useful tool to investigate treatment options for idiopathic pulmonary fibrosis? *Int. J. Biochem. Cell Biol.* **2008**, 40, 362–382. DOI: 10.1016/j.biocel.2007.08.011.
26. Latta, V.D.; Cecchettini, A.; Ry, S.D.; Morales, M.A. Bleomycin in the setting of lung fibrosis induction: From biological mechanisms to counteractions. *Pharmacol. Res.* **2015**, 97, 122–130. DOI: 10.1016/j.phrs.2015.04.012
27. Izbicki, G.; Segel, M.J.; Christensen, T.G.; Conner, M.W.; Breuer, R. Time course of bleomycin-induced lung fibrosis. *Int. J. Exp. Pathol.* **2002**, 83, 111–119. DOI: 10.1046/j.1365-2613.2002.00220.x
28. Fernandez, I.E.; Amarie, O.V.; Mutze, K.; Königshoff, M.; Yildirim, A.Ö.; Eickelberg, O. Systematic phenotyping and correlation of biomarkers with lung function and histology in lung fibrosis. *Am. J. Physiol. Lung Cell Mol. Physiol*. **2016**, 310, L919–927. DOI: 10.1152/ajplung.00183.2015

29. Selman, M.; Pardo, A. Role of epithelial cells in idiopathic pulmonary fibrosis: from innocent targets to serial killers. *Proc. Am. Thorac. Soc.* **2006**, 3, 364–372. DOI: 10.1513/pats.200601-003TK
30. Yoshida, K.; Kuwano, K.; Hagimoto, N.; Watanabe, K.; Matsuba, T.; Fujita, M.; Inoshima, I.; Hara, N. MAP kinase activation and apoptosis in lung tissues from patients with idiopathic pulmonary fibrosis. *J. Pathol.* **2002**, 198, 388–396. DOI: 10.1002/path.1208
31. Ventura, J.J.; Tenbaum, S.; Perdiguero, E.; Huth, M.; Guerra, C.; Barbacid, M.; Pasparakis, M.; Nebreda, A.R. p38alpha MAP kinase is essential in lung stem and progenitor cell proliferation and differentiation. *Nat. Genet.* **2007**, 39, 750–758. DOI: 10.1038/ng2037
32. Kolahian, S.; Fernandez, I.E.; Eickelberg, O.; Hartl, D. Immune Mechanisms in Pulmonary Fibrosis. *Am. J. Respir. Cell Mol. Biol.* **2016**, 55, 309–322. DOI: 10.1165/rcmb.2016-0121TR
33. Bakin, A.V.; Rinehart, C.; Tomlinson, A.K.; Arteaga, C.L. p38 mitogen-activated protein kinase is required for TGFbeta-mediated fibroblastic transdifferentiation and cell migration. *J. Cell Sci.* **2002**, 115, 3193–3206.
34. Khalil, N.; Xu, Y.D.; O'Connor, R.; Duronio, V. Proliferation of pulmonary interstitial fibroblasts is mediated by transforming growth factor-beta1-induced release of extracellular fibroblast growth factor-2 and phosphorylation of p38 MAPK and JNK. *J. Biol. Chem.* **2005**, 280, 43000–43009. DOI: 10.1074/jbc.M510441200
35. Kolosova, I.; Nethery, D.; Kern, J.A. Role of Smad2/3 and p38 MAP kinase in TGF-β1-induced epithelial-mesenchymal transition of pulmonary epithelial cells. *J. Cell Physiol.* **2011**, 226, 1248–1254. DOI: 10.1002/jcp.22448
36. Lee, C.G.; Homer, R.J.; Zhu, Z.; Lanone, S.; Wang, X.; Koteliansky, V.; Shipley, J.M.; Gotwals, P.; Noble, P.; Chen, Q.; et al. Interleukin-13 induces tissue fibrosis by

selectively stimulating and activating transforming growth factor β1. *J. Exp. Med.* **2001**, 194, 809–822. DOI: 10.1084/jem.194.6.809

37. Mi, S.; Li, Z.; Yang, H.Z.; Liu, H.; Wang, J.P.; Ma, Y.G.; Wang, X.X.; Liu, H.Z.; Sun, W.; Hu, Z.W. Blocking IL-17A promotes the resolution of pulmonary inflammation and fibrosis via TGF-beta1-dependent and -independent mechanisms. *J. Immunol.* **2011**, 187, 3003–3014. DOI: 10.4049/jimmunol.1004081
38. Passalacqua, G.; Mincarini, M.; Colombo, D.; Troisi, G.; Marta Ferrari, M.; Bagnasco, D.; Balbi, F.; Riccio, A.; Canonica, G.W. IL-13 and idiopathic pulmonary fibrosis: Possible links and new therapeutic strategies. *Pulm. Pharmacol. Ther.* **2017**, 45, 95–100. DOI: 10.1016/j.pupt.2017.05.007
39. Gurczynski, S.J.; Moore, B.B. IL-17 in the lung: the good, the bad, and the ugly. *Am. J. Physiol. Lung Cell Mol. Physiol.* **2018**, 314, L6–L16. DOI: 10.1152/ajplung.00344.2017
40. Nuovo, G.J.; Hagood, J.S.; Magro, C.M.; Chin, N.; Kapil, R.; Davis, L.; Marsh, C.B.; Folcik, V.A. The distribution of immunomodulatory cells in the lungs of patients with idiopathic pulmonary fibrosis. *Mod. Pathol.* **2012**, 25, 416–433. DOI: 10.1038/modpathol.2011.166
41. Xu, Y.; Mizuno, T.; Sridharan, A.; Du, Y.; Guo, M.; Tang, J.; Wikenheiser-Brokamp, K.A.; Perl, A.T.; Funari, V.A.; Gokey, J.J.; et al. Single-cell RNA sequencing identifies diverse roles of epithelial cells in idiopathic pulmonary fibrosis. *JCI Insight.* **2016**, 1, e90558. DOI: 10.1172/jci.insight.90558
42. Korfei, M.; Ruppert, C.; Mahavadi, P.; Henneke, I.; Markart, P.; Koch, M.; Lang, G.; Fink, L.; Bohle, R.M. Seeger, W.; et al. Epithelial endoplasmic reticulum stress and apoptosis in sporadic idiopathic pulmonary fibrosis. *Am. J. Respir. Crit. Care Med.* **2008**, 178, 838–846. DOI: 10.1164/rccm.200802-313OC
43. Hotamisligil, G.S.; Davis, R.J. Cell signaling and stress responses. *Cold Spring Harb. Perspect. Biol.* **2016**, 8, a006072. DOI: 10.1101/cshperspect.a006072

44. Liang, J.; Zhang, Y.; Xie, T.; Liu, N.; Chen, H.; Geng, Y.; Kurkciyan, A.; Mena, J.M.; Stripp, B.R.; Jiang, D.; et al. Hyaluronan and TLR4 promote surfactant-protein-C-positive alveolar progenitor cell renewal and prevent severe pulmonary fibrosis in mice. *Nat. Med.* **2016**, 22, 1285–1293. DOI: 10.1038/nm.4192

45. Schinzel, R.T.; Higuchi-Sanabria, R.; Shalem, O.; Moehle, E.A.; Webster, B.M.; Joe, L.; Bar-Ziv, R.; Frankino, P.A.; Durieux, J.; Pender, C.; et al. The hyaluronidase, TMEM2, promotes ER homeostasis and longevity independent of the UPR ER. *Cell.* **2019**, 179, 1306–1318, e18. DOI: 10.1016/j.cell.2019.10.018

46. Liang, J.; Liu, N.; Liu, X.; Mena, J.M.; Xie, T.; Geng, Y.; Huan, C.; Zhang, Y.; Taghavifar, F.; Huang, G.; et al. Mitogen-activated protein kinase-activated protein kinase 2 inhibition attenuates fibroblast invasion and severe lung fibrosis. *Am. J. Respir. Cell Mol. Biol.* **2019**, 60, 41–48. DOI: 10.1165/rcmb.2018-0033OC

47. Craig, V.J.; Zhang, L.; Hagood, J.S.; Owen, C.A. Matrix metalloproteinases as therapeutic targets for idiopathic pulmonary fibrosis. *Am. J. Respir. Cell Mol. Biol.* **2015**, 53. 585–600. DOI: 10.1165/rcmb.2015-0020TR

48. Darling, T.K.; Lamb, T.J. Emerging roles for Eph receptors and ephrin ligands in immunity. *Front. Immunol.* **2019**, 10, 1473. DOI: 10.3389/fimmu.2019.01473

49. Habiel, D.M.; Espindola, M.S.; Jones, I.C.; Coelho, A.L.; Stripp, B.; Hogaboam C.M. CCR10+ epithelial cells from idiopathic pulmonary fibrosis lungs drive remodeling. *JCI Insight.* **2018**, 3, e122211. DOI: 10.1172/jci.insight.122211

50. Mohan, T.; Deng, L.; Wang, B.Z. CCL28 chemokine: An anchoring point bridging innate and adaptive immunity. *Int. Immunopharmacol.* **2017**, 51, 165–170. DOI: 10.1016/j.intimp.2017.08.012

51. Zhou, H.; Brekman, A.; Zuo, W.L.; Ou, X.; Shaykhiev, R.; Agosto-Perez, F.J.; Wang, R.; Walters, M.S.; Salit, J.; Strulovici-Barel, Y.; et al. POU2AF1 Functions in the human

airway epithelium to regulate expression of host defense genes. *J. Immunol.* **2016**, 196, 3159–3167. DOI: 10.4049/jimmunol.1502400

52. Sun, X.; Hou, T.; Cheung, E.; Iu, T.N.; Tam, V.W.; Chu, I.M.; Tsang, M.S.; Chan, P.K.; Lam, C.W.; Wong. C. Anti-inflammatory mechanisms of the novel cytokine interleukin-38 in allergic asthma. *Cell Mol. Immunol.* **2020**, 17, 631–646. DOI: 10.1038/s41423-019-0300-7
53. McDonough, J.E.; Ahangari, F.; Li, Q.; Jain, S.; Verleden, S.E.; Herazo-Maya, J.; Vukmirovic, M.; DeIuliis, G.; Tzouvelekis, A.; Tanabe, N.; et al. Transcriptional regulatory model of fibrosis progression in the human lung. *JCI Insight.* **2019**, 4, e131597. DOI: 10.1172/jci.insight.131597
54. Du, Y.; Guo, M.; Whitsett, J.A.; Xu, Y. 'LungGENS': a web-based tool for mapping single-cell gene expression in the developing lung. *Thorax.* **2015**, 70, 1092–1094. DOI: 10.1136/thoraxjnl-2015-207035
55. de Vries, M.; Faiz, A.; Woldhuis, R.R.; Postma, D.S.; de Jong, T.V.; Sin, D.D.; Bossé, Y.; Nickle, D.C.; Guryev, V.; Timens, W.; et al. Lung tissue gene-expression signature for the ageing lung in COPD. *Thorax.* **2017**, thoraxjnl-2017-210074. DOI: 10.1136/thoraxjnl-2017-210074
56. Brosh, R.; Sarig, R.; Natan, E.B.; Molchadsky, A.; Madar, S.; Bornstein, C.; Buganim, Y.; Shapira, T.; Goldfinger, N.; Paus, R.; et al. p53-dependent transcriptional regulation of EDA2R and its involvement in chemotherapy-induced hair loss. *FEBS Lett.* **2010**, 584, 2473–2477. DOI: 10.1016/j.febslet.2010.04.058
57. Sisto, M.; Lorusso, L.; Lisi, S. X-linked ectodermal dysplasia receptor (XEDAR) gene silencing prevents caspase-3-mediated apoptosis in Sjögren's syndrome. *Clin. Exp. Med.* **2017**, 17, 111–119. DOI: 10.1007/s10238-015-0404-z
58. Yamada, H.; Yanagisawa, K.; Tokumaru, S.; Taguchi, A.; Nimura, Y.; Osada, H.; Nagino, M.; Takahashi, T. Detailed characterization of a homozygously deleted region

corresponding to a candidate tumor suppressor locus at 21q11-21 in human lung cancer. *Genes Chromosomes Cancer*. **2008**, 47, 810–818. DOI: 10.1002/gcc.20582

59. Zhu, Y.X.; Benn, S.; Li, Z.H.; Wei, E.; Masih-Khan, E.; Trieu, Y.; Bali, M.; McGlade, C.J.; Claudio, J.O.; Stewart, A.K. The SH3–SAM adaptor HACS1 is up-regulated in B cell activation signaling cascades. *J. Exp. Med.* **2004**, 200, 737–747. DOI: 10.1084/jem.20031816
60. DePianto, D.J.; Chandriani, S.; Abbas, A.R.; Jia, G.; N'Diaye, E.N.; Caplazi, P.; Kauder, S.E.; Biswas, S.; Karnik, S.K.; Ha, C.; et al. Heterogeneous gene expression signatures correspond to distinct lung pathologies and biomarkers of disease severity in idiopathic pulmonary fibrosis. *Thorax.* **2015**, 70, 48–56. DOI: 10.1136/thoraxjnl-2013-204596
61. Sivakumar, P.; Thompson, J.R.; Ammar, R.; Porteous, M.; McCoubrey, C.; Cantu, III, E.; Ravi, K.; Zhang, Y.; Luo, Y.; Streltsov, D.; et al. RNA sequencing of transplant-stage idiopathic pulmonary fibrosis lung reveals unique pathway regulation. *ERJ Open Res.* **2019**, 5, 00117-2019. DOI: 10.1183/23120541.00117-2019
62. Tanaka, K.; Fujita, T.; Umezawa, H.; Namiki, K.; Yoshioka, K.; Hagihara, M.; Sudo, T.; Kimura, S.; Tatsumi, T.; Kasuya, Y. Therapeutic effect of lung mixed culture-derived epithelial cells on lung fibrosis. *Lab. Invest.* **2014,** *94*, 1247–1259. DOI: 10.1038/labinvest.2014.109
63. Amano, H.; Murata, K.; Matsunaga, H.; Tanaka, K.; Yoshioka, K.; Kobayashi, T,; Ishida, I.; Fukamizu, A.; Sugiyama, F.; Sudo, T.; et al. p38 Mitogen-activated protein kinase accelerates emphysema in mouse model of chronic obstructive pulmonary disease. *J. Recept. Signal Transduct.* **2014**, *34*, 299–306. DOI: 10.3109/10799893.2014.896380
64. Hubner, R.H.; Gitter, W.; El Mokhtari, N.E.; Mathiak, M.; Both, M.; Bolte, H.; Freitag-Wolf, S.; Bewig, B. Standardized quantification of pulmonary fibrosis in histological samples. *Biotechniques*. **2008**, *44*, 507–511. 514-7. doi: 10.2144/000112729

65. Wang, X.; Inoue, S.; Gu, J.; Miyoshi, E.; Noda, K.; Li, W.; Mizuno-Horikawa, Y.; Nakano, M.; Asahi, M.; Takahashi, M.; et al. Dysregulation of TGF-beta1 receptor activation leads to abnormal lung development and emphysema-like phenotype in core fucose-deficient mice. *Proc. Natl. Acad. Sci. U S A.* **2005**, *102*, 15791–15796. DOI: 10.1073/pnas.0507375102

66. Maruyama, M.; Sudo, T.; Kasuya, Y.; Shiga, T.; Hu, B.; Osada, H. Immunolocalization of p38 MAP kinase in mouse brain. *Brain Res.* **2000**, 887, 350-358. doi: 10.1016/s0006-8993(00)03063-8

67. Ohkuro, M.; Kim, JD.; Kuboi, Y.; Hayashi, Y.; Mizukami, H.; Kobayashi-Kuramochi, H.; Muramoto, K.; Shirato, M.; Michikawa-Tanaka, F.; Moriya, J.; et al. Calreticulin and integrin alpha dissociation induces anti-inflammatory programming in animal models of inflammatory bowel disease. *Nat. Commun.* **2018**, *9*, 1982. DOI: 10.1038/s41467-018-04420-4

68. Subramanian, A.; Tamayo, P.; Mootha, V.K.; Mukherjee, S.; Ebert, B.L.; Gillette, M.A.; Paulovich, A.; Pomeroy, S.L.; Golub, T.R.; Lander, E.S.; et al. Gene set enrichment analysis: a knowledge-based approach for interpreting genome-wide expression profiles. *Proc. Natl. Acad. Sci. U S A.* **2005**, *102*, 15545–15550. DOI: 10.1073/pnas.0506580102

69. Ge, S.X.; Son, E.W.; Yao, R. iDEP: An integrated web application for differential expression and pathway analysis of RNA-Seq data. *BMC Bioinform.* **2018**, *19*, 534. DOI: 10.1186/s12859-018-2486-6

70. Chen, J.; Bardes, E.E.; Aronow, B.J.; Jegga, A.G. ToppGene Suite for gene list enrichment analysis and candidate gene prioritization. *Nucleic Acids Res*. **2009**, *37*, W305–W311. DOI: 10.1093/nar/gkp427

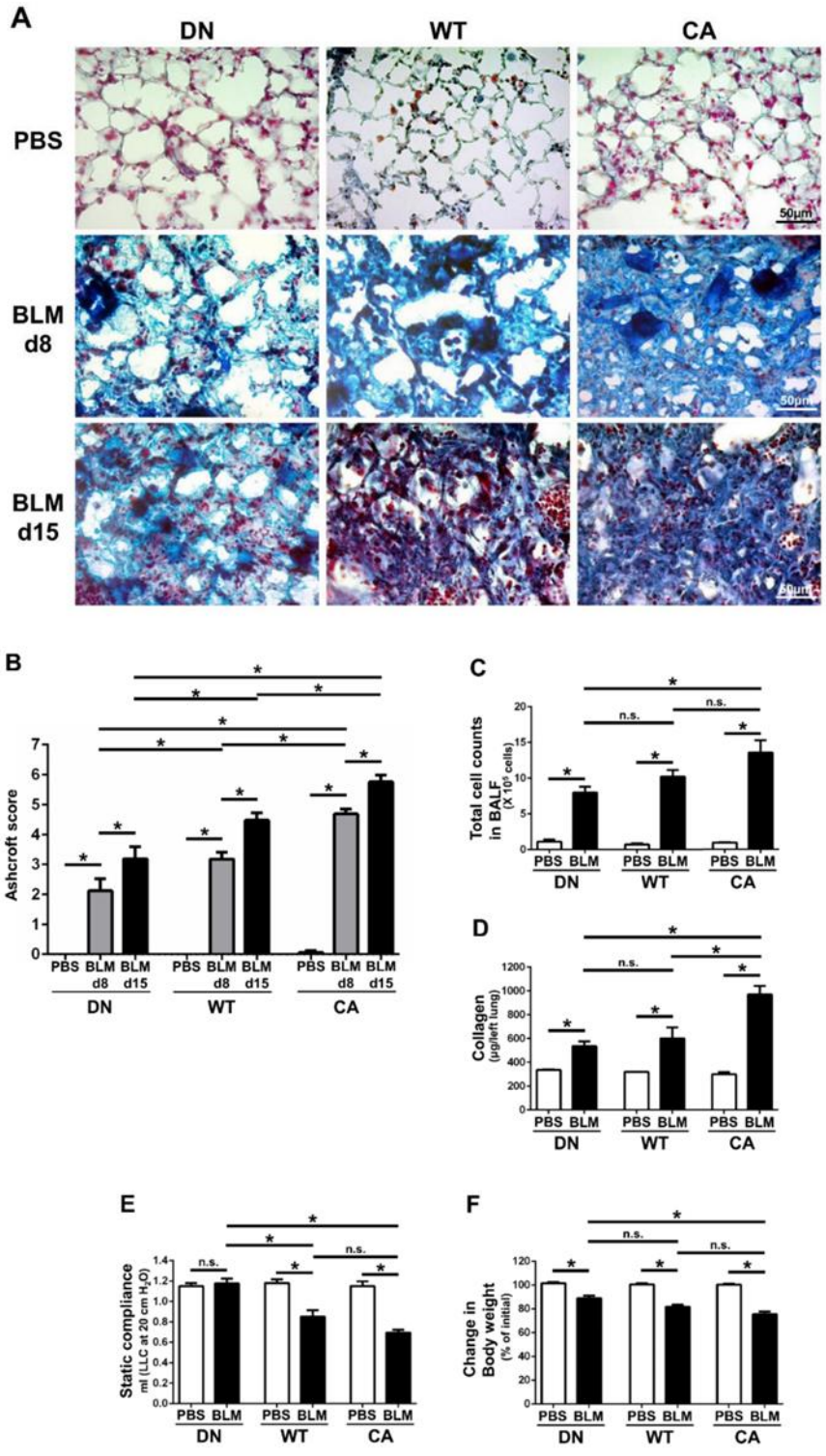

Figure 1. Bleomycin (BLM)-induced pulmonary fibrosis in mice bearing three different abilities of p38 in the lungs. The three mouse genotype groups; namely, MKK6 constitutive active group (CA), wild type group (WT), and p38 dominant negative group (DN), were intratracheally administrated BLM and phosphate-buffered saline (PBS). (**A**) Representative

histopathological images of the lung sections stained by Masson's trichrome (scale bar = 50 μm). Lungs were collected at 8 days post-instillation (dpi) of BLM and PBS, and 15 dpi of BLM. (**B**) Quantification of the fibrotic severity using modified Ashcroft scoring was evaluated in six different lesions at 8 dpi of BLM and PBS, and 15 dpi of BLM (n = 9). (**C**) The numbers of total cells in bronchoalveolar lavage fluid were measured at 8 dpi of BLM and PBS (n = 7). (**D**) The collagen contents of the left lung lobes were measured at 8 dpi of BLM and PBS and normalized to the weight of each left lung (n = 4). (**E**) The static lung compliances were measured at 8 dpi of BLM and PBS (n = 4). (**F**) Proportions of body weight at 8 dpi of BLM and PBS to that before administration (n = 14). All data are represented as means ± standard error of the mean (SEM). * $p < 0.05$, n.s., no significant difference (measured by one-way an analysis of variance (ANOVA) followed by Tukey's test or unpaired Student's *t*-test).

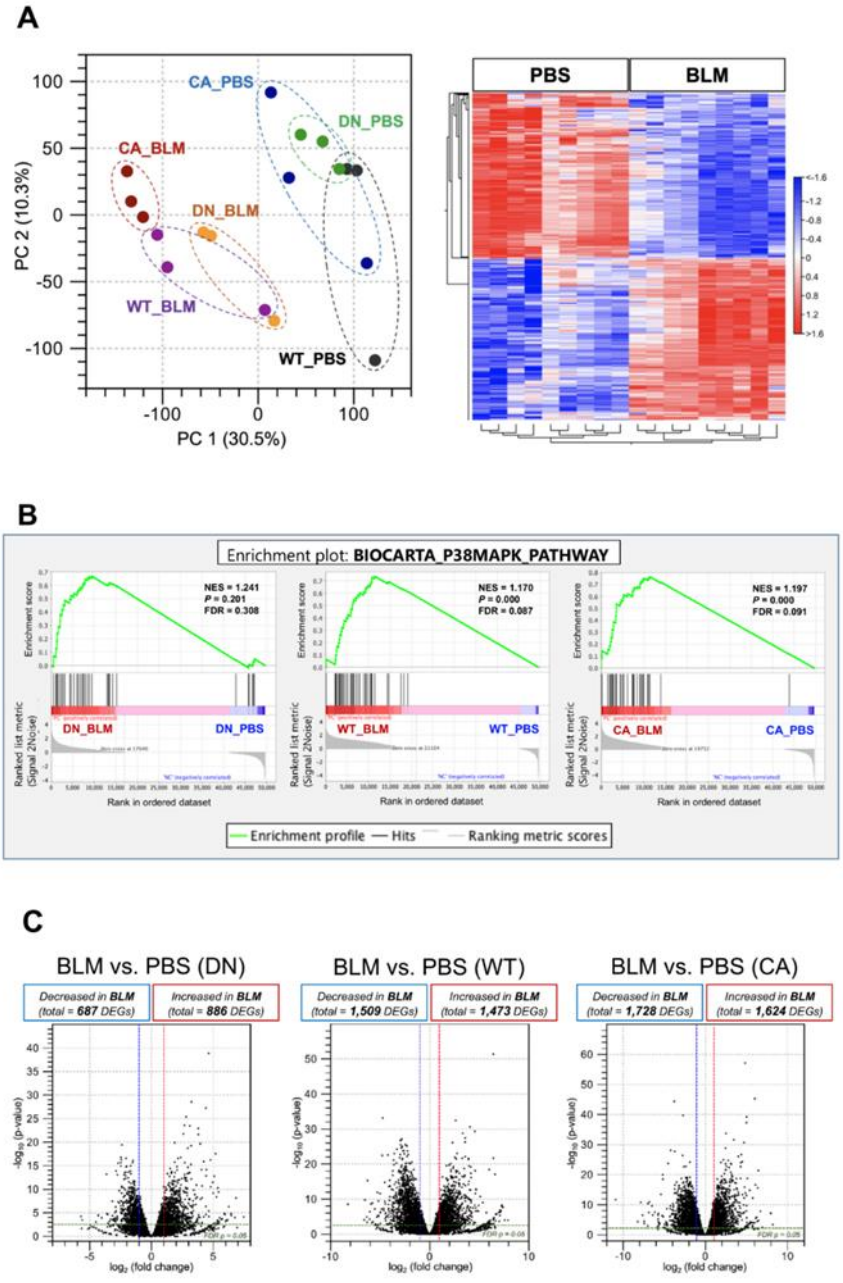

Figure 2. Expression profiling of BLM- and PBS-treated lungs in three different mouse genotypes. Three samples from each group were sequenced. (**A**) Principal component analysis of RNA sequencing datasets among the BLM- and PBS-treated three mouse groups (left). Hierarchical clustering shown in a heatmap of gene expression profiles between the BLM- and PBS-treated groups (right). The red and blue strips represent upregulated and downregulated genes in each group, respectively. (**B**) Gene set enrichment analysis of differential expression in the p38 MAPK pathway between the BLM- and PBS-treated groups of three mouse genotypes. The normalized enrichment scores (NES), normal *p*-values, and

false discovery rate (FDR) q values are indicated. (**C**) Volcano plot of differentially expressed genes altered by BLM treatment among three mouse groups. Upregulated and downregulated genes are discriminated based on log2 fold-change and adjusted FDR *p*-value (<0.05).

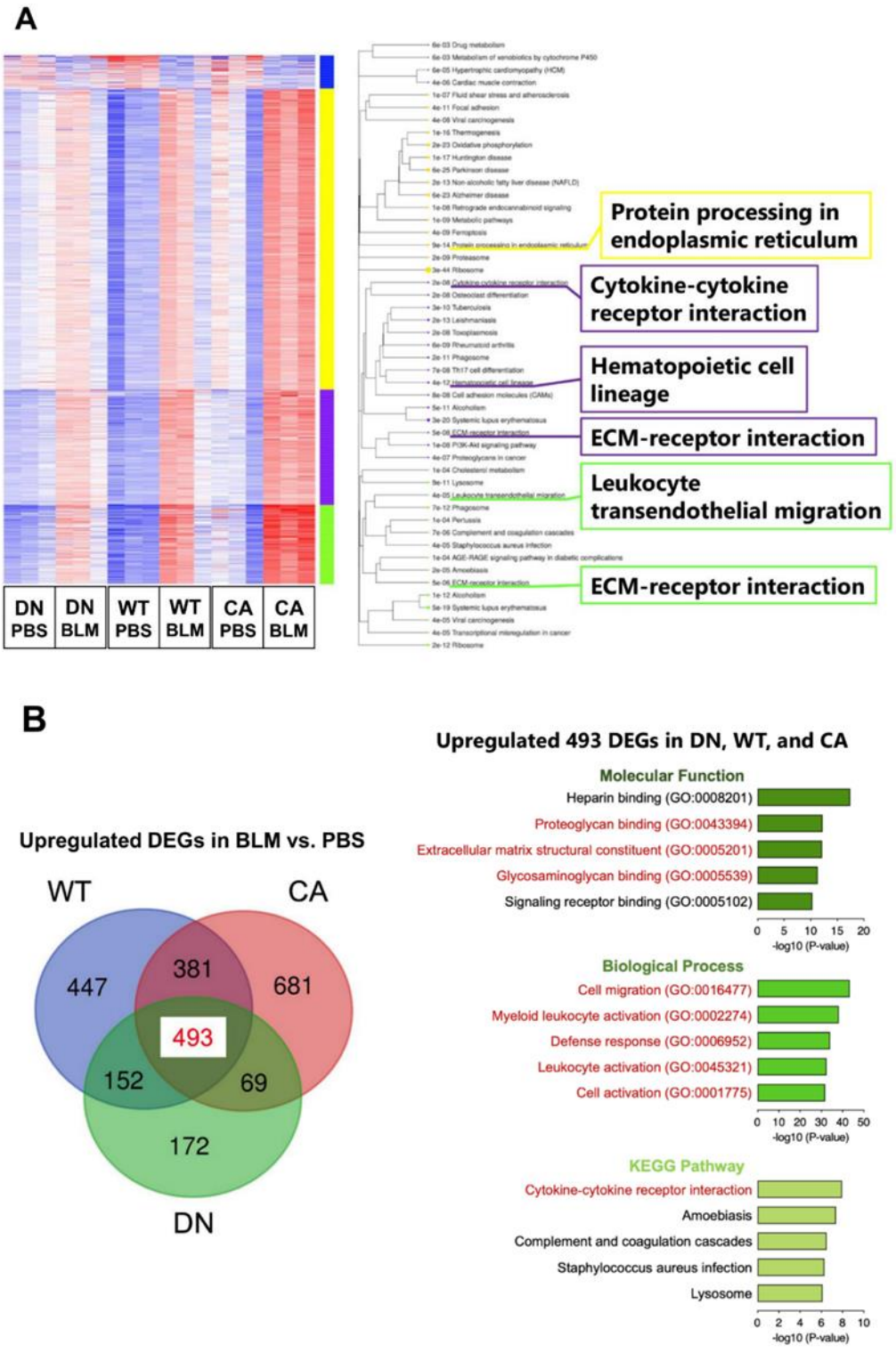

Figure 3. Gene ontology (GO) and Kyoto Encyclopedia of Genes and Genomes (KEGG) pathway enrichment analysis of differentially expressed genes (DEGs) altered by BLM treatment among three mouse groups. (**A**) K-means clustering shown in a heatmap based on the gene expression profiles between the BLM- and PBS-treated groups of three mouse

genotypes (left). The colored bars on the right of the diagram indicate clusters. The trees represent enriched KEGG pathways corresponding to each cluster (right). (**B**) Venn diagram showing the overlap of DEGs upregulated by BLM among three mouse groups, with the numbers of DEGs indicated in each area (left). GO and KEGG pathway enrichment analysis of 493 common upregulated DEGs among the three genotypes (right). Top five enriched GO terms associated with molecular function (upper) and biological process (middle), and KEGG pathway analysis (bottom).

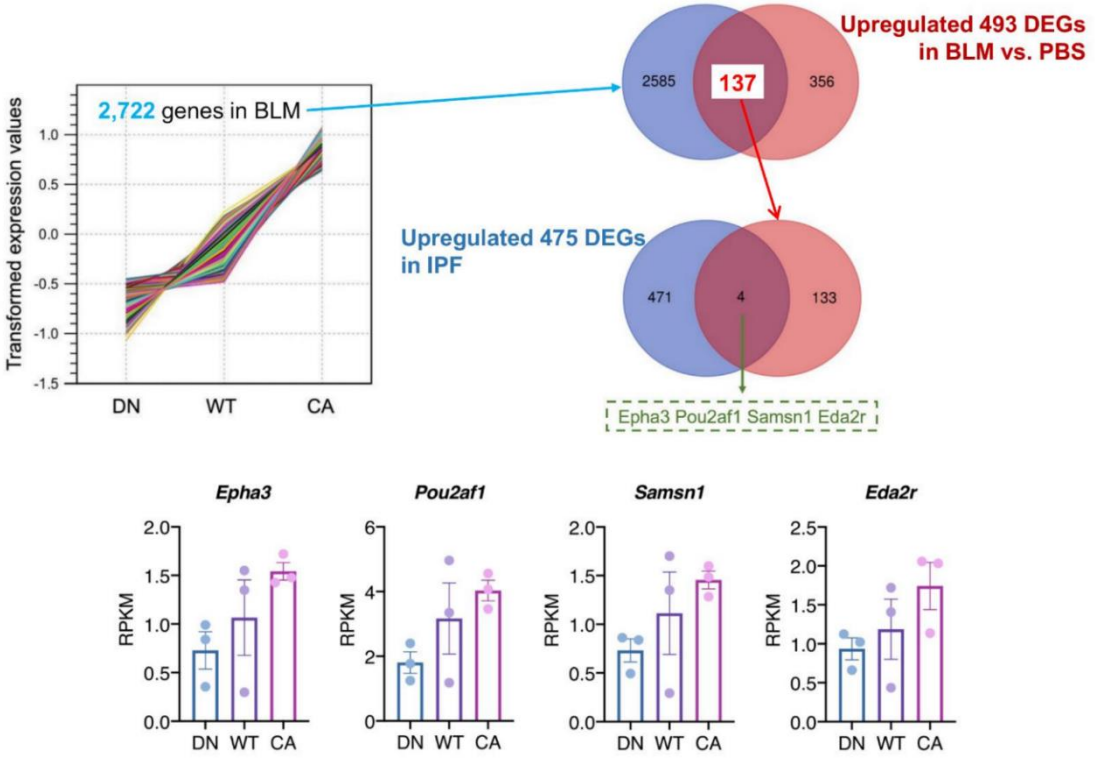

Figure 4. Identification of potential target genes by comparison to a publicly available idiopathic pulmonary fibrosis (IPF) dataset. K-means cluster analysis among three mouse groups treated with BLM revealed a cluster of 2722 genes showing correlation between variations of their mean expression values and stepwise changes in intrinsic p38 activity in the lungs (**left upper**). The Venn diagram in the right upper tier shows the overlap of 2722 genes in this cluster and 493 common upregulated DEGs among the three mouse groups. Likewise, the Venn diagram in the right middle tier shows the overlap of 137 genes identified in our study and 475 upregulated DEGs in human IPF lungs from dataset GSE52463. The four overlapping genes identified in these analyses were EPH receptor A3 (*EPHA3*), POU class 2 homeobox associating factor 1 (*POU2AF1*), SAM domain, SH3 domain and nuclear localization signals 1 (*SAMSN1*), and ectodysplasin A2 receptor (*EDA2R*) (**bottom**). Each bar and plot represent mean reads per kilobase of exon per million mapped sequence reads (RPKM) ± SEM and RPKM value of each sample, respectively.

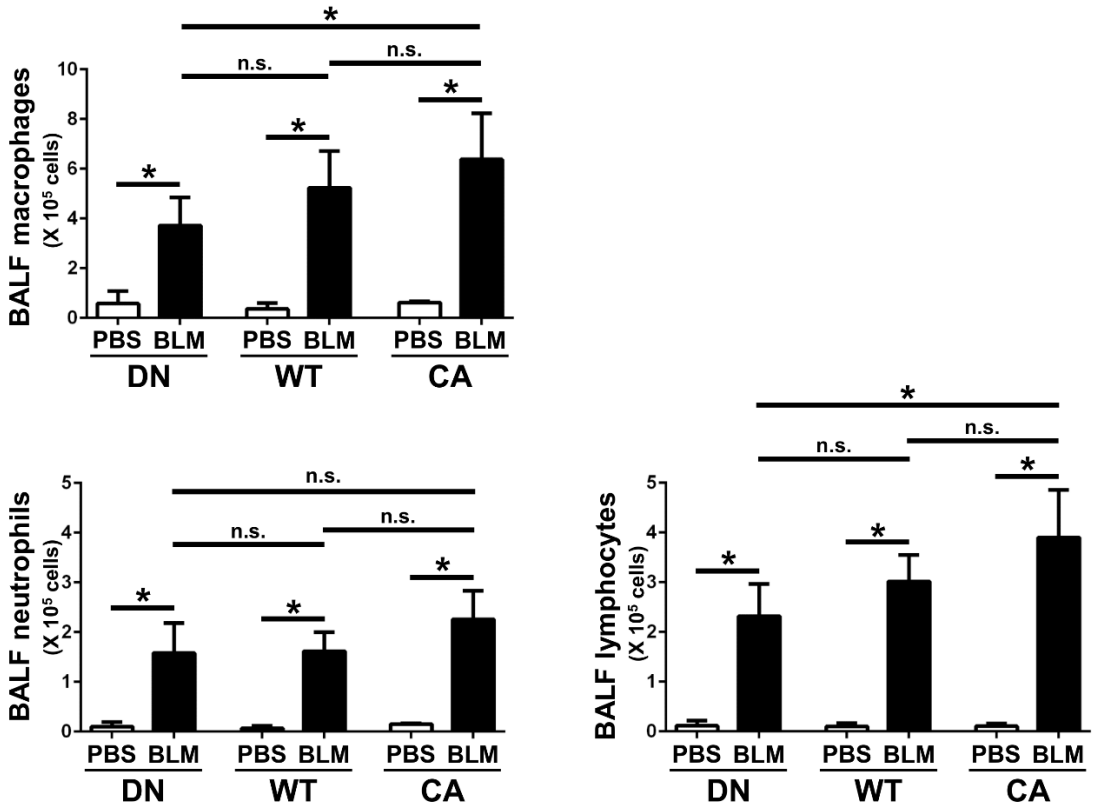

Supplementary Figure S1. Differential cell counts in BALF. The numbers of macrophages, lymphocytes, and neutrophils in BALF at 8 dpi of BLM and PBS were compared among three mouse groups. Data are represented as means ± SEM (n = 5). *$p < 0.05$, n.s., no significant difference (measured by one-way ANOVA followed by Tukey's test or unpaired Student's t-test).

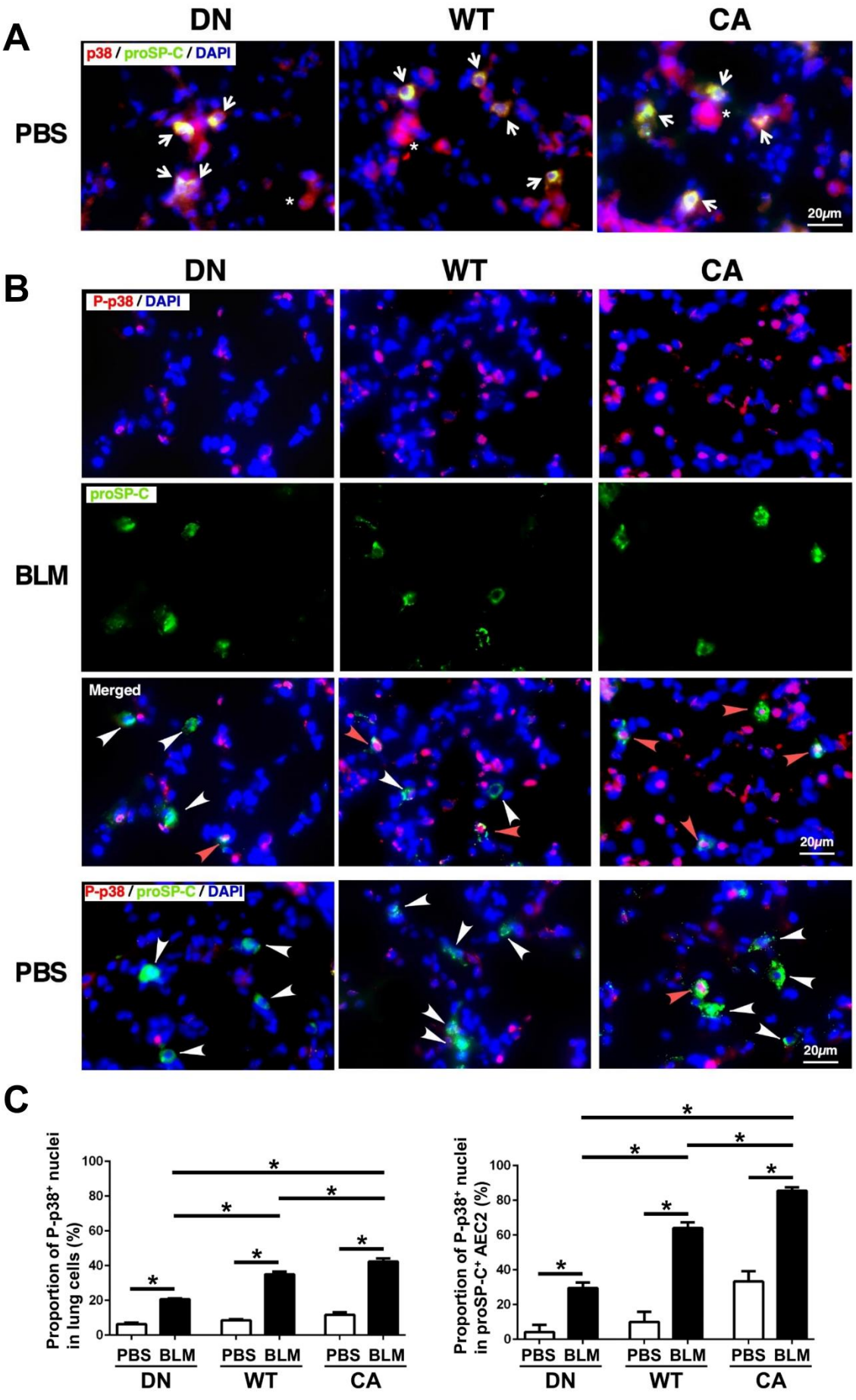
A
DN
WT
CA
PBS
p38 / proSP-C / DAPI
20μm
B
DN
WT
CA
P-p38 / DAPI
BLM
proSP-C
Merged
20μm
PBS
P-p38 / proSP-C / DAPI
20μm
C
Proportion of P-p38+ nuclei in lung cells (%)
100
80
60
40
20
0
PBS BLM PBS BLM PBS BLM
DN WT CA
Proportion of P-p38+ nuclei in proSP-C+ AEC2 (%)
100
80
60
40
20
0
PBS BLM PBS BLM PBS BLM
DN WT CA

Supplementary Figure S2. The expression and activity of p38 in the lungs with different genotypes. The three mouse genotype groups; DN, WT and CA, were intratracheally administrated PBS and BLM. (**A**) The lung sections of the PBS-treated groups at 8 dpi were subjected to immunofluorescence staining for p38 (red) and prosurfactant protein-C (proSP-C, green). DAPI (blue) stains nuclei. Arrows indicate $p38^+$ proSP-C^+ cells. Asterisks indicate alveolar macrophages. Among the three mouse genotypes, the lung distribution of p38 expression was almost unchanged in alveolar epithelial type II cells (AEC II), macrophages, and some other parenchymal cells. (**B**) The lung sections of the BLM- and PBS-treated groups at 8 dpi were subjected to immunofluorescence staining for phospho-p38 (P-p38, red) and proSP-C (green). DAPI (blue) stains nuclei. Arrow heads indicate SP-C^+ cells. In particular, red arrow heads indicate SP-C^+ cells with P-$p38^+$ nuclei, revealing p38 activation in AEC II. Few AEC II showed P-$p38^+$ nuclei in the PBS-treated DN and WT groups, while modestly increased number of them were observed in the PBS-treated CA group. Additionally, the number of AEC II with P-$p38^+$ nuclei was increased in the BLM-treated groups as compared with the PBS groups in all genotypes. At least in AEC II, BLM-induced stepwise activation of p38 was dependent on the genetically modified intrinsic p38 activity. (**C**) Proportion of nuclear localization of P-p38 in lung cells and AEC II. To quantify BLM-induced phosphorylation/nuclear translocation of p38, the ratio of P-p38-positive nuclei to total DAPI-positive nuclei, and proSP-C-positive cells with P-p38-positive nuclei to all proSP-C-positive cells were evaluated in 4 random fields (1.7mm^2 each per field) under fluorescence microscopy (400× magnification). Data are represented as means ± SEM. *p < 0.05, n.s., no significant difference (measured by one-way ANOVA followed by Tukey's test or unpaired Student's t-test).

Supplementary Table S1. BLM-induced cytokine molecules in BALF that were correlated with intrinsic p38 activity in the lungs.

Pro-fibrotic cytokines	Induction Index (Arbitary unit)		
Name	DN	WT	CA
IL-13	5.2	6.5	15.0
IL-17	8.5	32.2	43.5
SDF-1/CXCL12	2.9	5.4	7.2

Pro-inflammatory mediators	Induction Index (Arbitary unit)		
Name	DN	WT	CA
CCL1/TCA-3	2.5	5.8	6.8
Eotaxin/CCL11	4.0	39.0	62.0
IFN-γ	6.7	8.6	14.2
IL-15	3.5	6.0	14.0
KC/CXCL1	5.8	7.6	11.7
LIX/CXCL5	2.2	2.7	4.3
MIG/CXCL9	2.9	5.0	11.9
MIP-1α/CCL3	17.6	29.0	33.6
MIP-2/CXCL2	3.5	5.2	6.4
RANTES/CCL5	37.4	49.0	65.7
Thymus chemokine-1/CXCL7	1.4	2.8	5.4

Fibrosis-related proteins	Induction Index (Arbitary unit)		
Name	DN	WT	CA
Activin A	1.3	2.4	4.2
CXCL14	3.1	10.4	11.6
IGFBP-2	4.3	5.8	8.3
IGFBP-3	4.2	5.6	8.1
IGFBP-5	2.3	26.6	64.1
IL-22	11.0	26.0	49.0
MMP-2	3.7	6.5	9.4
MMP-3	15.0	41.0	88.2
MMP-9	4.0	17.0	93.7

Others	Induction Index (Arbitary unit)		
Name	DN	WT	CA
Cardiotrophin-1	7.5	30.0	42.5
CCL28	6.1	13.3	16.4
CCR9	2.7	3.5	5.5
CD11b	3.2	4.1	6.4
CD27 Ligand	3.5	6.7	8.6
IL-2R γ	9.7	17.3	23.1
CTACK	3.5	9.3	10.4
Dtk	2.5	3.9	5.3
EGF R	11.3	30.6	39.7
EG-VEGF	10.7	14.0	20.7
Endogrin/CD105	4.2	18.8	27.2
Eotaxin-2	10.2	31.6	34.3
FGF R3	6.7	8.6	15.2
Follistatin	1.2	3.8	8.1
Frizzled-1	1.2	4.9	8.5

GDF-5	28.5	47.5	61.0
GDF-8	27.8	46.7	65.9
GDF-9	9.0	33.0	42.0
GDNF Rα-2	1.7	24.0	58.0
IFN-γ R1	3.4	4.3	6.7
IGFBP-1	3.6	5.0	8.0
IGFBP-6	5.0	29.0	43.5
IL-1 RII	4.4	7.4	10.2
IL-3 Rα	8.3	86.4	113.6
IL-15 Rα	2.3	3.9	6.0
IL-16	4.6	7.5	10.1
IL-23 R	2.1	2.8	3.9
Kremen-1	4.9	17.4	28.3
Lungkine/CXCL15	3.2	4.0	5.8
Lymphotoxin βR	3.8	4.9	7.3
MAdCAM-1	5.7	18.7	25.7
MDC/CCL22	14.5	19.5	43.5
Osteoactivin	2.4	3.3	5.9
Osteoporotegerin	29.0	44.0	81.5
PDGF C	4.7	9.5	13.0
PDGF Rα	4.4	6.3	8.2
PIGF 2	5.0	14.3	22.7
Prolactin	2.3	3.2	4.6
P-selectin	2.2	2.7	4.1
Resistin	13.4	20.6	29.6
SIGIRR	3.5	24.5	32.3
Soggy-1	1.3	3.5	4.8
Spinesin Ectodomain	1.6	2.0	4.5
TGF-β3	6.0	22.1	35.6
TGF-β RII	2.5	3.5	4.7
TIMP-2	4.1	6.7	7.8
TIMP-4	24.1	44.1	52.7
TLiA/TNFSF15	6.7	16.0	31.0
TNF RI	1.9	6.8	13.1
TNF-β	1.5	3.6	5.7
TRANCE/TNFSF11	8.8	19.0	36.0
TWEAK	30.0	62.0	70.0
TWEAK R	2.9	4.0	4.9
WIF-1	15.3	34.7	57.3

Supplemenary Table S2. The gene symbol list of 493 common DEGs upregulated by BLM among MKK6-CA, WT, and p38-DN groups.

A2m	Ccl22	Clec5a	Ereg	Gyg
Abcb1b	Ccl6	Clec7a	Esco2	H2-Eb2
Ackr1	Ccl7	Cmah	Espl1	Has2
Ackr3	Ccl9	Cmtm3	Etv4	Havcr2
Adam12	Ccna2	Col12a1	F10	Hbegf
Adamts12	Ccnb2	Col28a1	F7	Hcn1
Adamts4	Ccne1	Col3a1	Fabp5	Hells
Adgre1	Ccnf	Col4a1	Fam105a	Hexb
AI506816	Ccng1	Col5a2	Fam20c	Hist1h1a
Ano5	Ccr1	Col5a3	Fam49b	Hist1h1b
Anxa1	Ccr2	Col8a1	Fbn1	Hist1h2ab
Aoah	Ccr5	Coro1a	Fcer1g	Hist1h2ak
Apbb1ip	Cd180	Cotl1	Fcgr1	Hist1h2bk
Apobec1	Cd200r1	Cpxm1	Fcgr2b	Hist1h2bm
Apoe	Cd200r4	Csf2rb	Fcgr3	Hist1h3d
Arg1	Cd248	Csf2rb2	Fcrls	Hist1h4f
Arhgdib	Cd276	Csmd1	Fermt3	Hpgds
Armcx4	Cd300a	Cstb	Fgr	Hsd17b7
Arpc1b	Cd300c2	Cthrc1	Fhl3	Hvcn1
Aspm	Cd300lf	Ctps	Fignl1	I830077J02Rik
Atg9b	Cd38	Ctsb	Fkbp10	Icam1
Atp1a3	Cd48	Ctsc	Fn1	Icos
Atp6v0c	Cd52	Ctsd	Foxm1	Ier3
Atp6v0d2	Cd53	Ctss	Frzb	Ifi204
B2m	Cd68	Ctsz	Fscn1	Ifi207
B3gnt5	Cd84	Cxcl10	Fst	Ifi209
B430306N03Rik	Cd86	Cxcl13	Fstl1	Ifi27l2a
Bard1	Cdc20	Cxcl15	Fzd1	Ifi30
Bcl2a1b	Cdca3	Cxcl16	Gas2l3	Ifit2
Bgn	Cdh11	Cxcl9	Gcnt4	Ifitm3
Birc5	Cdk1	Cybb	Gda	Igf1
Bmper	Cdkn1a	Cyp4f18	Gdf15	Igfbp2
Brinp1	Cemip	Cyp7b1	Gimap9	Igha
Bst1	Cenpf	Dab2	Gja1	Ighg2b
Btk	Cenpl	Dck	Gla	Ighv1-53
Btla	Cers6	Ddias	Glipr2	Ighv1-64
Bub1	Cfp	Dhfr	Glrx	Igkv10-96
C1qa	Ch25h	Diaph3	Gm10718	Igkv1-110
C1qb	Chl1	Disp2	Gm14548	Igkv1-117
C1qc	Chodl	Dlgap5	Gm6377	Igkv8-30
C1qtnf6	Chrna7	Ear2	Gnpda1	Iglc2
C330027C09Rik	Chsy3	Eda2r	Gpnmb	Igsf6
C3ar1	Ckap2	Egr2	Gpr141	Il1rn
C430002N11Rik	Ckap4	Eln	Gpr176	Il21r
C5ar1	Clca3a1	Emcn	Gpr35	Il2rg
Capg	Cldn4	Enc1	Gpr65	Il4ra
Capn6	Clec4a2	Eno1	Grn	Ildr2
Casp3	Clec4a3	Enpp1	Grrp1	Irf5
Ccdc80	Clec4e	Epha3	Gtse1	Isg15
Ccl17	Clec4n	Ercc6l	Gusb	Itga5

Itgam_1
Itgax
Itgb2
Itgb6
Itm2a
Kcnk13
Kctd12b
Kif11
Kif15
Kif22
Kif4
Knl1
Kntc1
Kynu
Lair1
Lama1
Lamb3
Lamc2
Laptm5
Lcn2
Lgals3
Lgals9
Lgmn
Lhfpl2
Lhx6
Lilrb4a
Lipa
Litaf
Lox
Loxl2
Lpcat2
Lpl
Lpxn
Lrg1
Lrp12
Lrp2
Lrrc25
Lrrc8c
Ltbp2
Ly6a
Ly6c1
Ly6c2
Ly86
Lyz2
Malt1
Map2
March1
Marcksl1
Mcemp1
Mcm5
Mdga1
Megf10
Mest
Mgp
Mki67
Mmp12
Mmp14
Mmp19
Mmp8
Mpeg1
Ms4a1
Ms4a6b
Ms4a6c
Ms4a6d
Ms4a7
Msr1
Mt2
Mthfd2
Mybl1
Myc
Myo5a
Naip2
Napsa
Ncapg
Ncapg2
Ncf2
Nckap1l
Ndc1
Ndnf
Nek6
Nfam1
Nme1
Nme2
Nos2
Nrcam
Nrep
Nt5e
Ntrk2
Nuf2
Nusap1
Nxpe4
Nxpe5
Oas3
Olfm1
Olr1
Osm
P2ry6
P4ha3
Pappa2
Pdgfc
Pdpn
Pgf
Phex
Phlda3
Pik3cg
Pilra
Pim1
Pirb
Pla1a
Plat
Plau
Plbd1
Pld3
Pld4
Plek
Plxnc1
Pole
Pou2af1
Ppa1
Prc1
Prcp
Prkcb
Prr11
Prrx2
Prss22
Psap
Psat1
Psmb8
Psrc1
Ptafr
Ptger4
Ptgir
Ptprc
Rab32
Rab3il1
Rab8b
Rac2
Racgap1
Rap2b
Rcan1
Rgs16
Rhoh
Rpl39
Rrm2
Rsad2
Rtn4rl2
S100a4
S100a6
Saa3
Samsn1
Sash3
Scarb1
Scn3b
Scube1
Sdcbp
Sdk2
Selp
Selplg
Serpina3g
Serpina3n
Serpinb6b
Serpinb9
Serpine1
Serpine2
Sfrp1
Sgk1
Sgpl1
Sh2b2
Sh2d1b1
Sh3pxd2b
Shc4
Shcbp1
Siglec1
Sirpa
Sirpb1c
Slamf9
Slc11a1
Slc15a3
Slc27a6
Slc29a3
Slc35f6
Slc37a2
Slc39a14
Slc7a8
Slfn1
Slfn10-ps
Slfn2
Slfn8
Slfn9
Sparc
Spc25
Spi1
Spp1
Sprr1a
Spry4
St8sia4
Stra6l
Svop
Syt12
Tfec
Tgfb1
Tgfbi
Tgm1
Thbs1
Thbs4
Tifab
Timp1
Tlr1
Tlr13
Tlr2
Tlr7
Tlr8
Tmem106a
Tmem173
Tmem26
Tmem37
Tmem86a
Tmsb10
Tnc
Tnfaip8l2
Tnfrsf11b
Tnfrsf12a
Tnfrsf13b
Tnfrsf1b
Tnfsf8
Tnip3
Top2a
Tpx2
Trem2
Trim59
Tspan8
Ttyh2
Tyrobp
Ubash3b
Ugcg
Ulbp1
Vcan
Vstm4
Wfdc17
Wisp1
Wnt10a
Wnt7a
Zfp385a

International Journal of Molecular Sciences Vol 21 No 18

2020 年 9 月 14 日　公表済

DOI: 10.3390/ijms21186746